Pressure effects on morphology of isotropic char layer, shrinkage, cracking and reduced heat transfer of wooden material

Kaiyuan Li, Yanyan Zou, Serge Bourbigot, Jie Ji, Xianfeng Chen

Pressure effects on morphology of isotropic char layer, shrinkage, cracking and reduced heat transfer of wooden material

Kaiyuan Li [a,d], Yanyan Zou [a], Serge Bourbigot [b], Jie Ji [c,*],
Xianfeng Chen [a,*]

[a] *School of Safety Science and Emergency Management, Wuhan University of Technology, Luoshi Road 122, Wuhan 430070, China*
[b] *Université Lille Nord de France, ENSCL, UMET/ISP R2Fire, Cité Scientifique-Bât C7-CS 90108, 59652 Villeneuve d'Ascq Cedex, France*
[c] *State Key Laboratory of Fire Science, University of Science and Technology of China, Hefei 230027, China*
[d] *BRANZ, Private Bag 50 908, Porirua 5240, New Zealand*

Abstract

Using a compartment with adjustable oxygen concentration and internal pressure, the shrinkage and cracking of isotropic char layer during pyrolysis were studied by pyrolyzing the medium density fibreboard (MDF) in inert atmosphere with different ambient pressures. The experimental results have shown that the ambient pressure has insignificant effect on shrinkage although some trends have been identified. Therefore, the reduction of tensile strength of material dominates the char cracking under low pressures, leading to noticeable increase in the number of char fissures. The char shrinkage could expose the raw material beneath the char layer and enhance the radiative heat transfer at the sample surface (by fissure width instead of number), which is modeled using a modified thermal conductivity as the typical simplification. It is found that the mass loss rate at the early pyrolysis stage increases up to 20% with increasing width of char fissures. However, the external radiation can only affect a limited depth in the near surface zone which is found less than 3 mm in the current experiments. The thermal conductivity under near regular pressure could be over 2 times higher than its value under low pressure (30 kPa) and with which the differences in the first peaks of mass loss rate under different pressures can be well predicted.

Keywords: Wood; Pyrolysis; Heat transfer; Pressure; Char

1. Introduction

Char layer has been found as an important thermal barrier blocking the external heat flux from

* Corresponding authors.
E-mail addresses: jijie232@ustc.edu.cn, stevelikai@126.com (J. Ji), cxf618@whut.edu.cn (X. Chen).

pyrolyzing the raw material of burning wood and other charring materials during combustion [1]. The "charring behaviors" including shrinkage and cracking induced by combustion can significantly affect the material pyrolysis, for instance, the char fissures induced by cracking will become important paths for heat transferred into the material and flame flowing out. Li et al. [2–5] investigated the charring behaviors of natural wood and wooden materials under regular pressure. However, these behaviors are still weakly implemented in the current modeling techniques [6–8] as the related research is not sufficient. Hence, to enhance the accuracy of combustion modeling, in-depth study should be carried out to reveal the effects of charring behaviors on the combustion process of wood and wooden materials, which make it possible to consider the behaviors of char layer in combustion and fire safety engineering.

In the past few decades, researchers have identified the charring behaviors of wood in regular conditions and reported in several different works [9–18]. Detail literature reviews have been conducted in the previous researches [2,3] therefore it is not repeated in this paper. As addressed previously, in the combustion process, the raw wood turns into porous media as part of the wood substance is gasified by pyrolysis reactions. The porous media usually has a lower inside pressure which causes the pressure difference between the internal space and surrounding environment, leading to char shrinkage. Moreover, unbalanced shrinkage led by different levels of pyrolysis across the sample depth results in char cracking and fissures. The theory of shrinkage cracking was first established from the drying processes in food and concrete industries [19,20]. The association between shrinkage and cracking has been identified [2,3]. Based on the hypothesis of shrinkage changing the ambient pressure might affect the char cracking behaviors. However, previous study [3] focused on the fracture mechanics of cracking under regular pressure without considering the effects of ambient pressure. In the past, most of the studies on the pressure effect have concentrated on the gas phase flame behaviors [21,22] in the combustion and fire community. There is a lack of research on the pressure effect on solid phase pyrolysis. Previous research has shown that the ambient pressure has ignorable effect on the chemical kinetics of pyrolysis [23]. Thus, the changes of thermo-physical properties and geometric deformations induced by pressure variations might strongly affect the charring behaviors. For instance, it has been found that as the ambient pressure increased the material tensile strength increased as the molecules become more compacted [24,25]. The change of tensile strength will significantly affect the char cracking. Besides, it has been pinpointed that the heat transfer is crucial to the pyrolysis of wood materials [26]. Therefore, the effects of charring behaviors on the
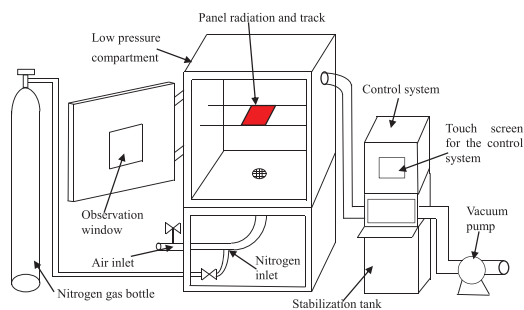

Fig. 1. Experimental apparatus [2].

heat transfer process should be addressed for the potential modification of numerical model.

To investigate the effects of ambient pressure on charring behavior and heat transfer, a number of MDF samples were pyrolyzed under different incident heat fluxes and ambient pressures. The MDF has an isotropic surface which simplifies the fire problem [27]. The mechanism of char cracking at different ambient pressures is revealed theoretically and moreover, the effects of charring behaviors on the heat transfer to the solid phase are discussed.

2. Experiments

2.1. Experiment facility

Figure 1 shows the configuration of the experiment facility [2]. A gas supply system with 2 pipes was used supplying both highly purified nitrogen and ambient air to a low-pressure compartment. A valve on each pipe controls the gas flowrate and thus the internal pressure and gas concentration in the compartment. The size of low-pressure compartment is 1.0 m (length) × 1.0 m (height) × 0.6 m (width). There is a 0.3 m square panel radiator inside the compartment pyrolyzing the samples with near uniform radiative heat fluxes. Digital camera was used to record the experiment processes. Apart from the regular experiments, a set of shrinkage experiments with two rulers as the holder were also conducted (refer to supplemental materials). In the shrinkage experiments, the real time vertical and horizontal shrinkages as well as the charring rate were measured. The experiments were controlled by a control system and more details can be found elsewhere [2,3].

2.2. Materials

The MDF samples were made of pine from mid-China. The bulk density of MDF panel is 730±17 kg/m^3 and the panel thickness is 15 mm. For general charring experiments, the sample size was 100 mm square while for those shrinkage experiments the sample size was 50 mm square (to reduce
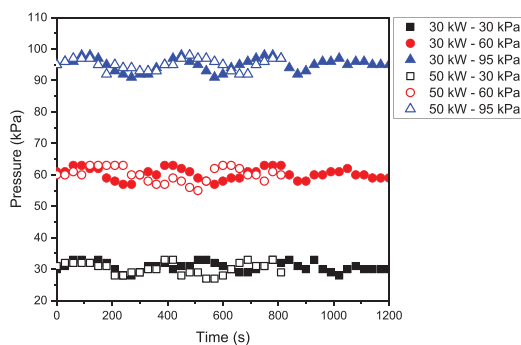
Fig. 2. Pressure records.

the smoke in the compartment). It should be noted that the moisture was removed from the MDF samples before the experiments.
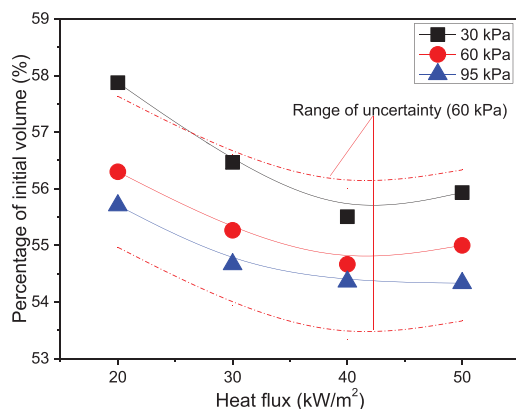
2.3. Experimental condition and procedure

The MDF samples were pyrolyzed under 3 ambient pressures (inside the compartment) of 95, 60, 30 kPa and 4 heat fluxes of 20, 30, 40, 50 kW/m². The nonuniformity of incident (radiative) heat flux was found less than 2.7% of the nominal value at the sample center for the 100 mm square area.

To simplify the problem, an inert atmosphere with pure nitrogen was created inside the low-pressure compartment by replacing the air with proper ventilation process, to avoid flaming and also the effects of flame on the samples during pyrolysis. The ambient pressure inside the compartment was adjusted by varying the amount of nitrogen in the compartment using simultaneously the gas supply system and vacuum pump shown in Fig. 1. Figure 2 presents the pressure records during the experiments. The experiment times are 2000s, 1300s, 1000s and 850 s for respective 20, 30, 40 and 50 kW/m². Each experiment will be repeated for 3 times to ensure the repeatability. The experimental error is found less than 10% for all measured variables and more details regarding the experimental procedure can be referred to Ref. [3].
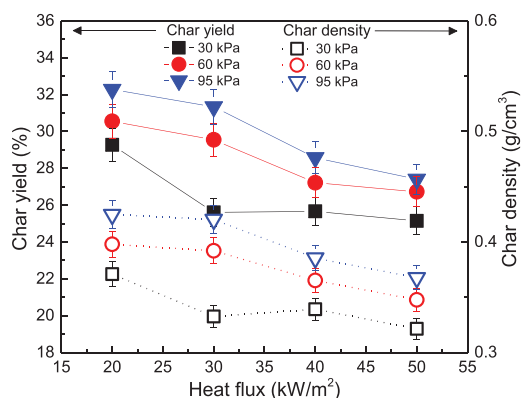
3. Results and discussion

3.1. Shrinkages, char densities and fissures at different ambient pressures

The sample began to char and produced pyrolysis gas when the panel radiator was turned on. There was no flame due to the lack of oxygen. The sample surface started turning into black in a few seconds with noticeable deformation and shrinkage observed. After a certain period of time, the sample cracked generating a lot of smoky gas. The char fissures then took place owing to cracking and in

(a) Char volume

(b) Char residue mass and density

Fig. 3. Measured char layer volume, char yield and density.

the current set of experiments it was found that the number of char fissures remained mostly the same during the whole process.
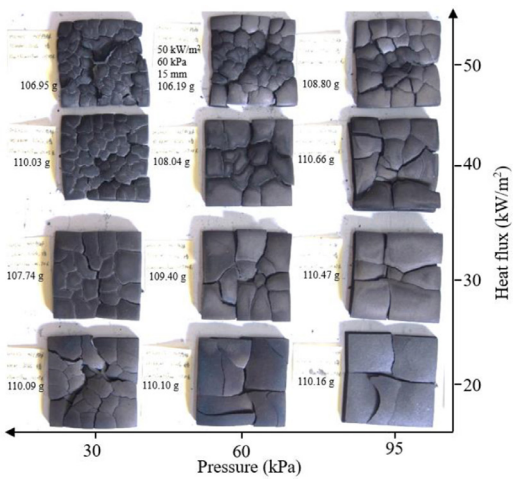
Figure 3 shows the char residue volume, mass and densities under different experimental conditions. We define the shrinkage ratio as shrunk length over original length. As reported previously [3], the shrinkage ratio at the vertical direction was measured as 30±2%, which is much higher than the one at the horizontal direction of 11±1%. In the literature, the longitudinal and tangential shrinkages of wood fibers are respective 3–8% and 12–15% [16]. As shown in the scanning electron microscope results in our previous work [3], the MDF is in fact made of layers of wood fibers randomly orientated in various directions. Therefore, the average value of longitudinal and tangential shrinkages of 7.5–11.5% can be expected for the horizontal shrinkage of MDF while the current measurement falls into this range. The vertical

shrinkage of MDF is caused by the interaction between wood fiber layers and there is no data to compare in the literature. However, in the current research we did both horizontally and vertically (supplemental materials) orientated experiment to confirm the shrinkage ratio. From the experiment, it is difficult to identify the pressure effect based on the shrinkage ratio. Although Fig. 3a shows that the char volume will drop with increasing heat flux and ambient pressure, it is seen that the variation is not able to fully overcome the uncertainty of measurement. Therefore, the char volume could be regarded as constant in the current study. Nevertheless, the differences in the measured mass of char residue under difference experimental conditions can be easily identified, as shown in Fig. 3b. From Fig. 3b, the char yield decreases with decreasing ambient pressure and increasing heat flux. Therefore, the same trend can be expected for the char density. It is understandable that when the heat flux increases more substance will be decomposed under higher temperature and heating rate [28,29], resulting in less residue. This is in line with the findings in the literature [28,29]. Meanwhile, it was found that increasing pressure increases the yields of char due to the increases of secondary reactions for microscale samples [30,31]. Therefore, the current finding is consistent with the previous researches, however, more bench-scale experiments are demanded for engineering applications.
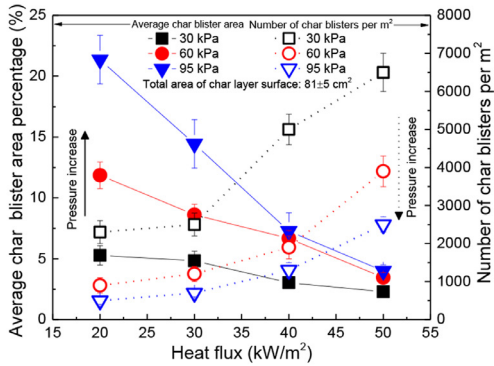
Figure 4a presents the photos of char fissure. From Fig. 4a, as the ambient pressure decreases and heat flux increases the number of fissures increases, indicating the enhanced extent of cracking. It should also be noted that there is boundary effect on cracking. As seen in Fig. 4a, the char blisters close to the sample edges are generally larger than those at the sample center, especially for high ambient pressures. For low ambient pressures, the sizes of char blisters are more even, such as the case under 30 kPa and 50 kW/m², indicating an early cracking time with weak shrinkage. The boundary effect is not involved in the current model. Figure 4b shows the number and average area of char blisters. From Fig. 4b, it is found that the number of char blisters increases while its average area decreases with decreasing ambient pressure and increasing heat flux. If the shape of the char blister is assumed as a square, the number of fissures at one direction on the surface can be approximated as

$$N_{30kPa} - 3 \approx N_{60kPa} - 1 \approx N_{95kPa} \quad (1)$$

where N is the number of char fissures, which can be determined using the square root of number of char blisters minus 1. Equation (1) is an empirical correlation from the experimental results and in the following section we will prove its validity through theoretical analysis.

(a) Char fissures

(b) Number and average area of char blisters

Fig. 4. Photo of char fissures and number and average area of char blisters.

3.2. Theoretical analysis on the number of char blisters

In our previous research under regular pressure [3], the mechanism of cracking initiation has been partly investigated, which could be caused by the thermal shock effect induced by pyrolysis shrinkage. In Ref. [3], the surface tensile stress of each char blister induced by unbalance shrinkage is calculated. This tensile stress should not exceed the surface tensile strength according to fracture mechanics. Otherwise, new crack takes place reducing the size of char blister. The detail derivation of cracking initiation equations can be found in [3]. The current paper uses the same mechanism as the one in Ref. [3]. However, as both size of char blister and surface tensile strength change under
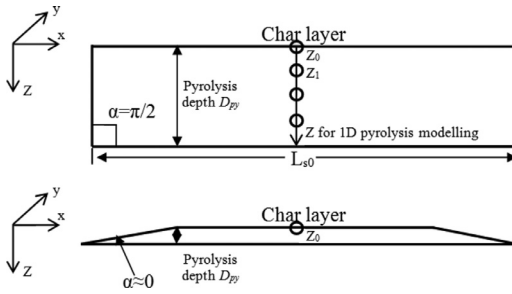
Fig. 5. Surface strains when the angle of relative shrinkage equals to $\pi/2$ and 0.

Fig. 6. Peak surface tensile stresses at different pressures ($\sigma_{s,peak}$ is determined using the measured data in Fig. 4).

low pressures, the surface tensile stress should be re-calculated. For isotropic shrinkage at the sample surface, the shrinkages at the two directions on the surface plane are identical therefore the surface stress is

$$\sigma_s = \frac{E\varepsilon_s}{1-\nu} \qquad (2)$$

where σ_s is the surface tensile stress, ε_s denotes the surface strain, ν is the Poisson ratio, E is the Young's modulus. The surface strain is a function of the angle of relative shrinkage, α [3]. As shown in Fig. 5, when α is near $\pi/2$, the surface strain is 0 (surface and lower materials have the same shrinkage) regardless of the deformation compared to raw material, whereas when it is close to 0, the surface strain is close to $\Delta L_{s0}/L_{s0}$. The surface strain can be expressed as

$$\varepsilon_s = C\left(\frac{\Delta L_{s0}}{L_{s0}}\right) = \frac{2\Delta D_{py}}{L_{s0}} ctg\alpha \qquad (3)$$

where C is the constant related to relative shrinkage, α is the angle led by relative shrinkage of char layer, D_{py} is the pyrolysis depth (m) which is defined as the distance from the sample surface to the location where raw material starts pyrolyzing, ΔL_{s0} is the length of shrinkage at the sample surface (m), L_{s0} is the original length of sample or char blister (m). Therefore,

$$\sigma_s \propto ctg\alpha \qquad (4)$$

Assuming the same shrinkage under different ambient pressures, as discussed above, the surface stress decreases when the number of char fissures increases, as the α increases. Then,

$$ctg\alpha \propto \frac{1}{N+1} \propto \sigma_s \leq \sigma_{critical} \qquad (5)$$

where $\sigma_{critical}$ is the surface tensile strength for cracking. Detailed analysis on the angle of relative shrinkage can be referred to Ref. [3]. However, it should be noted that Eq. (5) cannot be used to compare the stresses at different incident heat fluxes as the pyrolysis processes are different. Very little research has focused on the mechanical properties
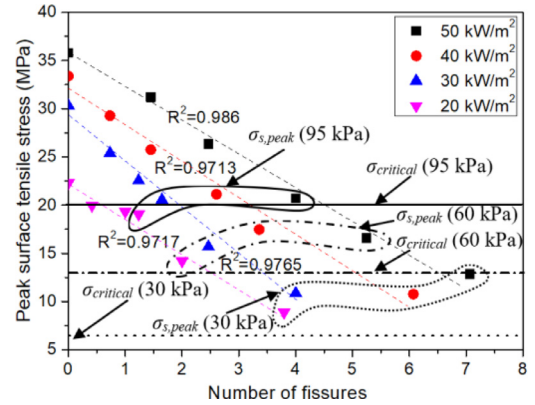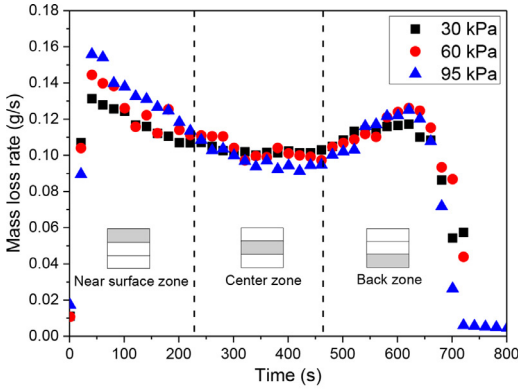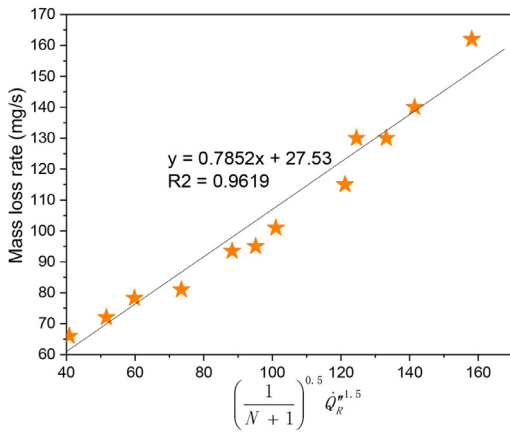
of wooden materials under different pressures. Wu et al. [32] conducted a set of measurements under different pressures for corn straw bio-board which has a lower tensile strength than MDF. It was found that the tensile strength of engineering board has a linear correlation with the pressure, which is

$$\sigma_{critical} \propto P \qquad (6)$$

where P is the ambient pressure, while the Young's modulus maintains nearly constant although at high pressures it might slightly decrease. One possible explanation for the trends of tensile strength and Young's modulus is that under high pressure the cross-linked structure of wood fibers is more compacted, enhancing its strength and stiffness. Using the numerical results in Ref. [3] and Eq. (5), the peak surface tensile stresses of char blister against the number of fissures under different heat fluxes are plotted in Fig. 6. From Fig. 6, it is seen that increasing the number of fissures reduces the surface tensile stress. According to the mechanism of shrinkage cracking, the number of fissures is mainly determined by the shrinkage during pyrolysis and the tensile strength of material. As the shrinkage under different pressures are similar, the tensile strength dominates the cracking and as it drops with decreasing pressure the peak surface tensile stress should also decrease. The decrease of stress can be seen in Fig. 6, as a result of tensile strength variation. However, although the peak surface tensile stresses are similar with different heat fluxes, the one of 20 kW/m² is generally lower than the others, which is mainly caused by the longer cracking time [3], leading to the failure of elastic assumption of MDF. Meanwhile, it is found that the calculated values, $\sigma_{s,peak}$, are systematically higher than the theoretical tensile strengths, $\sigma_{critical}$. This discrepancy could be a result of the uncertainties of Eq. (6), boundary effect and 2D model of stress. Therefore, future works with more accurate numerical simulations are demanded.

(a) 50 kW/m^2 mass loss rate

(b) Peak MLR against number of fissures and radiative heat flux

Fig. 7. Typical mass loss rate curves and correlation of peak MLR against N and $\dot{Q}''_R$.

3.3. Effects of char fissures on pyrolysis modeling

3.3.1. Mass loss rate

It has been long debated on the effect of fissure on the heat transfer during solid combustion in the community [33]. In theory, shrinkage and cracking will expose the raw material to the external heat fluxes in conduction, convection and radiation modes, therefore, enhance the heat transfer into the material. However, so far there is not any quantitative assessment on the effects of shrinkage cracking on heat transfer in the literature, perhaps due to the experimental difficulties. The current experiments lead to some new findings in this regard. Figure 7a shows the measured mass loss rates under 50 kW/m^2. As shown in Fig. 7a, it has been found that overall the mass loss rates at different pres-

sures are similar, however, the first peak of mass loss rate increases with increasing pressure. The difference of the first peaks at 30 and 95 kPa cases is approximately 20% which is much over the uncertainty of repeated experiments. Therefore, we can confirm that the first peaks of mass loss rate are different under different heat fluxes. Similar trends have been identified in other heat fluxes (supplemental materials). It should be noted that the major difference takes place at the early stage of mass loss rate curve while weak difference is identified in the curvatures and the second peaks. This implies that the heat transfer enhancement mainly affects the materials near the surface while the influences on the center and back zones are weak, as highlighted in Fig. 7a. The measured surface temperatures (refer to the Supplemental material) are another evidence proving the effects of char fissures on heat transfer, which are higher under lower pressures. This is reasonable as the radiation dominates the current pyrolysis process therefore it can be expected that both the radiative heat flux and view factor decrease as goes deep into the fissure, which reduces the effects of radiation enhancement. It should also be noted that due to the higher average sample temperature and the reduction of secondary reactions [30,31], the mass loss lasted longer at the late stage of experiment under low pressure (material pyrolyzes more completely), leading to low char residue mass as shown in Fig. 4b. For the near surface zone, the mass loss rate is determined by the radiative heat flux $\dot{Q}''_R$ and the heat transfer process affected by the fissures. Under the same shrinkage, the amount of radiative heat flux penetrating the fissure is determined by the area of fissure which increases with increasing $ctg\alpha$ and decreasing N, which is

$$A_{fissure} \propto ctg\alpha \propto \frac{1}{N+1} \quad (7)$$

In the current paper, we proposed a simple way for correlating the first peak of mass loss rate with the radiative heat flux $\dot{Q}''_R$ and number of fissures N. Figure 7b summarizes the measured first peaks and fitting result which is

$$\dot{m} \propto \left(\frac{1}{N+1}\right)^{0.5} \dot{Q}''_R{}^{1.5} \quad (8)$$

where $\dot{m}$ is the first peak of mass loss rate. Equation (8) is empirical and it should be noted that both kinetics and heat transfer determine $\dot{m}$, however, since MDF is identical the heat transfer dominates the change of $\dot{m}$ in this work. The first peak takes place when the char layer effect is weak therefore it is related to the depth of char layer [2,3] which increases with thermal conductivity and heating time using semi-infinite solid hypothesis as [2,34]

$$\dot{m} \propto \delta_p \propto \sqrt{k_s t} \quad (9)$$

where k_s is the solid thermal conductivity and t is the time to first peak of mass loss rate which has a correlation with the radiative heat flux as [35]

$$t \propto \frac{1}{\dot{Q}''_R{}^2} \qquad (10)$$

Therefore, combining Eqs. (8)–(10) gives

$$\sqrt{\frac{k_s}{\dot{Q}''_R}} \propto \sqrt{\frac{1}{N+1}} \dot{Q}''_R{}^2 \qquad (11)$$

As k_s is a material property, in Eq. (11) it only relates to the number of fissures, which gives

$$k_s \propto \frac{1}{N+1} \qquad (12)$$

From Eq. (12), under the same incident heat flux, the thermal conductivity has a linear trend with $1/(N+1)$ (refer to supplemental material for the limitation of Eq. (12)). With this principle, the thermal conductivities of both raw material and char are simultaneously modified in the near surface zone and numerical simulations are carried out to view the effect of thermal conductivity modification.

3.3.2. Solid phase pyrolysis model

The current work uses a pyrolysis model that solves the pyrolysis process of material using a set of 1D mesh taking into account the chemical kinetics and physical heat transfer simultaneously. The transport process of pyrolysis gas within the solid was neglected. A general pyrolysis gas was generated at the same temperature as the local solid, and was assumed to leave the solid phase instantaneously.
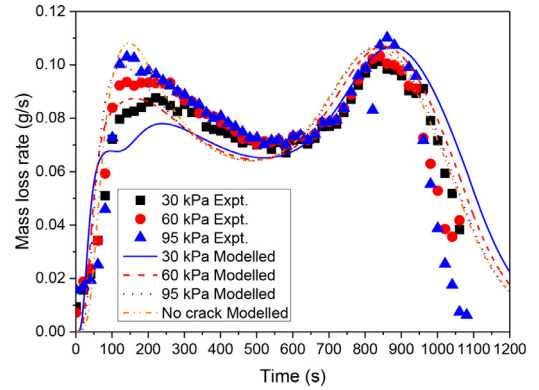
3.3.3. Kinetics and thermo-physical properties

In the previous works, a set of thermogravimetric (TG) experiments were conducted under multiple heating rates, based on which a non-first-order ($n \neq 1$) kinetic model with 4 parallel reactions of four components (resin, hemicellulose, cellulose, and lignin) was proposed for MDF [3]. The kinetics properties, initial mass fractions and char yields were determined using genetic algorithm previously [3]. In the pyrolysis model, the average thermal conductivity of solid phase was calculated in the volumetric basis as
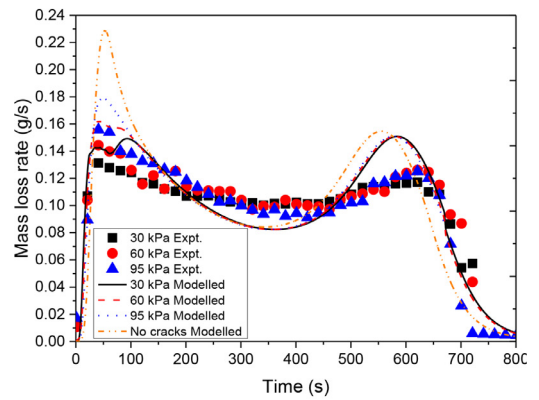
$$k_s = \bar{\rho} \sum_{i=1}^{N} \left(\frac{Z_i}{\rho_i} k_i \right) \qquad (13)$$

and it changes with the local density. The average specific heat capacity of solid phase was estimated based on the masses of components as

$$c_s = \sum_{i=1}^{N} Z_i c_i \qquad (14)$$

(a) 30 kW/m^2

(b) 50 kW/m^2

Fig. 8. Modeling results with modified thermal conductivities in the near surface zone.

3.3.4. Modeling results

Using Eq. (12), the modified thermal conductivity was assigned to near surface zone and the typical modeling results are shown in Fig. 8. It can be seen that with the modified thermal conductivities the first peak of mass loss rate noticeably drops as the ambient pressure decreases from 95 to 30 kPa, while the rest mass loss rates maintain nearly identical between different pressures. The modeled results match the experiments better at 30 kW/m^2 while the model over-predicts the mass loss peaks and under-predicts the curvature at 50 kW/m^2. From the trial and error process, it is found that the depth of the modified thermal conductivity zone should be within 1 to 3 mm. It should also be noted that from the current set of experiments the thermal conductivity under 95 kPa could be over 2 times higher than its value under 30 kPa (20 kW/m^2 case).

4. Conclusions

Char shrinkage and cracking and their effects on the heat transfer during pyrolysis are investigated using isotropic wooden surface under varied ambient pressures. It is found that the pressure has some effect on the char shrinkage however it is insignificant compared to the decrease of tensile strength with decreasing pressure. As a result, the char layer shrinkage creates more fissures under low pressures compared to regular pressure. It also indicates that the pressure difference between interior space of char layer and ambient environment may not be the main mechanism leading to shrinkage. The experimental result shows that as the number of char fissures increases the peak mass loss rate decreases. The increase of char fissures reduces the fissure width (area) induced by horizontal shrinkage, which could weaken the radiation heat transfer into the sample. By modifying the thermal conductivity of near surface zone, the numerical model can reproduce the different first peaks of mass loss rates at the early pyrolysis stage. However, the modeling results show that the zone affected by cracking is less than 3 mm in the current experiments and the thermal conductivity under near regular pressure could be 2 times higher than its value under low pressure.

Declaration of Competing Interest

The authors declare that they have no known competing financial interests or personal relationships that could have appeared to influence the work reported in this paper.

Acknowledgment

Supplementary materials

1. MLR data under 20 and 40 kW/m^2.
2. Detail derivation of thermal conductivity equation and an example in FDS model.
3. Shrinkage experiment of MDF samples with different orientations.
4. Measured surface and center temperature data under 30 and 50 kW/m^2.

Supplementary material associated with this article can be found, in the online version, at doi:10.1016/j.proci.2020.07.072.

References

[1] C. Di Blasi, *Prog. Energy Combust.* 34 (2008) 47–49.
[2] K.Y. Li, S. Hostikka, P. Dai, Y. Li, H. Zhang, J. Ji, *Proc. Combust. Inst.* 36 (2017) 3185–3194.
[3] K.Y. Li, M. Mousavi, S. Hostikka, *Fire Saf. J.* 91 (2017) 165–173.
[4] K.Y. Li, X. Cheng, H. Zhang, *Fire Mater.* 38 (2014) 659–672.
[5] K. Li, D.S.W. Pau, J. Wang, J. Ji, *Chem. Eng. Sci.* 123 (2015) 39–48.
[6] K. McGrattan, S. Hostikka, R. McDermott, J. Floyd, C. Weinschenk, *Fire Dynamics Simulator, Technical Reference Guide, Volume 1: Mathematical Model*, NIST Special Publication, 2015 1018-1.
[7] J. Li, J. Gong, S.I. Stoliarov, *Int. J. Heat Mass Transf.* 77 (2014) 738–744.
[8] C. Lautenberger, C. Fernandez-Pello, *Combust. Flame* 156 (2009) 1503–1513.
[9] A.F. Roberts, *Combust. Flame* 17 (1971) 79–86.
[10] M.J. Spearpoint, Predicting the Ignition and Burning Rate of Wood in the Cone Calorimeter Using an Integral Mode, NIST GCR 99-975, 1999.
[11] H.C. Tran, R.H. White, *Fire Mater.* 16 (1992) 197–206.
[12] K.O. Davidsson, J.B.C. Pettersson, *Fuel* 81 (2002) 263–270.
[13] J.B. Zicherman, R.B. Williamson, *Wood Sci. Technol.* 15 (1981) 237–249.
[14] T.J. Haas, M.R. Nimlos, B.S. Donohoe, *Energy Fuel* 23 (2009) 3810–3817.
[15] M.S. Gilani, J.L. Fife, M.N. Boone, K.G. Wakili, *Wood Sci. Technol.* 47 (2013) 889–896.
[16] Q. Liu, D. Shen, R. Xiao, M. Fang, *Combust. Sci. Technol.* 185 (2013) 848–862.
[17] M.J. Hagge, K.M. Bryden, *Chem. Eng. Sci.* 57 (2002) 2811–2823.
[18] D.K. Shen, S. Gu, K.H. Luo, A.V. Bridgwater., *Energy Fuel.* 23 (2009) 1081–1088.
[19] Z.C. Grasley, D.A. Lange, *Cem. Concr. Aggreg.* 26 (2004) 115–122.
[20] L. Mayor, A.M. Sereno, *J. Food Eng.* 61 (2004) 373–386.
[21] M. Zarzecki, J.G. Quintiere, R.E. Lyon, T. Rossmann, F.J. Die, *Combust. Flame* 160 (2013) 1519–1530.
[22] R.F. McAlevy, R.S. Magee, *Proc. Combust. Inst.* 12 (1969) 215–227.
[23] Y. Wang, X. Zheng, *J. Fire Sci.* 31 (2013) 495–510.
[24] P.W. Bridgman, *Rev. Mod. Phys.* 17 (1945) 3–14.
[25] T.V. Parry, A.S. Wronski, *J. Mater. Sci.* 20 (1985) 2141–2147.
[26] F. Richter, A. Atreya, P. Kotsovinos, G. Rein, *Proc. Combust. Inst.* 37 (2019) 4053–4061, doi:10.1016/j.proci.2018.06.080.
[27] D. Zeinali, S. Verstockt, T. Beji, G. Maragkos, J. Degroote, B. Merci, *Combust. Flame* 189 (2018) 491–505.
[28] E.M. Suuberg, I. Milosavljevic, W.D. Lilly, Behavior of Charring Materials in Simulated Fire Environments, NIST GCR 94-645, 1994.

[29] P.H. Brunner, P.V. Roberts, *Carbon* 18 (1980) 217–224.
[30] W.S.L. Mok, M.J. Antal, *Thermochim. Acta* 68 (1983) 155–164.
[31] F. Shafizadeh, *J. Anal. Appl. Pyrol.* 3 (1982) 283–305.
[32] T. Wu, X. Wang, K. Kito, *Eng. Agric. Environ. Food* 8 (2015) 123–129.
[33] A.F. Roberts, *Proc. Combust. Inst.* 13 (1971) 893–903.
[34] A. Atreya, I.S. Wichman, *J. Heat Transf.* 111 (1989) 719–725.
[35] K.Y. Li, D.S.W. Pau, J.H. Wang, J. Ji, *Chem. Eng. Sci.* 123 (2015) 39–48.